International Journal of Research
(IJR)
p-ISSN: 2348-6848
e-ISSN: 2348-795X
Vol. 8 Issue 12
December 2021

A Progressive High Gain DC DC Converter Applied For Fuel Cell Vehicles In Transportation Applications

Ajjuboyini Mahesh[1], Dr. A.Mallikarjuna Prasad[2]
[1]P.G. Scholar, [2]Guide, Head of the Department
[1,2] BRANCH :M.TECH(P& ID)
[1,2] Geethanjali College Of Engineering And Technology, Kurnool.
Email.Id : [1]maheshbunny9966@gmail.com, [2]mallikarjunaprasad0307@gmail.com

ABSTRACT

For fuel cell vehicles, the DC-DC converter should have a high gain, low voltage stress, small size, and high efficiency. Conventional two-level, three-level, and cascaded boost converters, on the other hand, are unable to match the requirements. This work proposes a new non-isolated DC-DC converter with switched-capacitor and switched-inductor, which has a high gain, a wide input voltage range, low voltage stresses between components, and a common ground topology. The operating principle, component parameter design, and comparisons with other high-gain converters are all discussed in this paper. To obtain the dynamic model of the converter, the state-space averaging method and small-signal modelling method are used. Finally, simulation and experimental data back-up the proposed topology's usefulness. The experimental prototype's input voltage varies from 25 to 80 volts. The rated output voltage is 200V, with a 100W rated power. Under the rated state, the maximum efficiency is 93.1 percent. Fuel cell vehicles can use the suggested converter.

INTRODUCTION

Structure of a fuel cell vehicle

The development of the transportation industry plays a vital role in the national economy. However, an increase in the number of fuel vehicles not only consumes a large amount of oil resources, but also causes serious environmental pollution problems. Therefore, all countries turn their attention to clean energy. The development of the new energy vehicle industry provides new ideas to solve these problems. Fuel cell vehicles have become a very promising development direction in the new energy vehicle industry due to its advantages of zero emissions, no pollution and high efficiency. The typical system structure of a fuel cell vehicle is shown in Fig. 1.1 The low output voltage of the fuel cell makes it difficult to meet the demand of DC bus voltage in front of the inverter. Moreover, the fuel cell has a "soft" output voltage characteristic, i.e., the output voltage drops too fast with the increase of the output current. Therefore, the DC-DC converter with high-gain, wide input voltage range and small size should be applied to fuel cell vehicles to raise the fuel cell voltage to a higher voltage level and ensure the stability of the DC bus voltage.

p-ISSN: 2348-6848
e-ISSN: 2348-795X
Vol. 8 Issue 12
December 2021

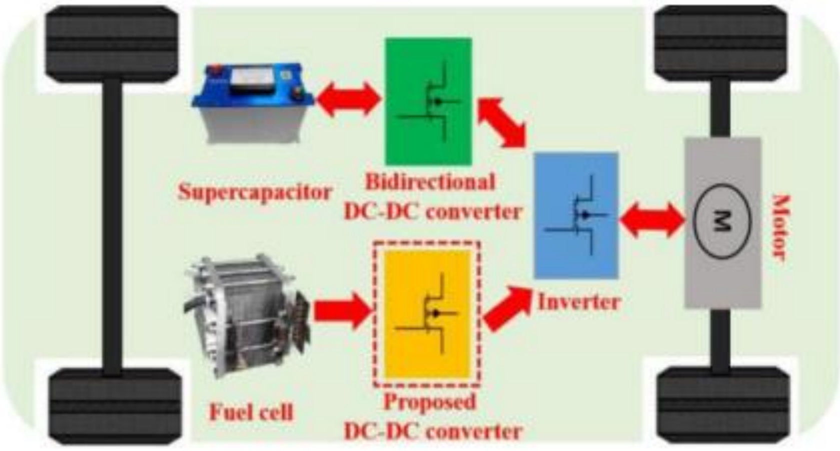

Fig.1.1 The typical system structure of a fuel cell vehicle

Isolated DC-DC converter can easily achieve high-gain by changing the transformer turns ratio. However, due to the leakage inductance of the transformer, the circuit will produce a peak voltage, which is easy to break down the devices in the circuit. The leakage inductance can also reduce the efficiency of the converter and cause electromagnetic interference problems. In addition, the transformer in the isolated converter also increases the size of the converter. Considering the size, cost and efficiency, the non-isolated DC-DC converter is more suitable for fuel cell vehicles. The traditional boost DC-DC converter is still used in many applications because of the small number of components and simple structure. The theoretical voltage gain of the boost converter is $1/(1-d)$, where d is the duty cycle of the drive voltage for the power switch. However, the voltage gain is limited due to the parasitic parameters of the actual circuit and components. The voltage stresses across components in the circuit are also high, which needs more expensive high-voltage components, resulting in increased size and cost. In addition, there is an extreme duty cycle in traditional boost converters when achieving high-gain, which causes serious diode reverse recovery problems, resulting in increased losses. In terms of these disadvantages, conventional boost converters are not suitable for fuel cell vehicles. The cascaded boost converter can achieve high-gain and wide input voltage range by sacrificing the overall power density and efficiency of the converter, but the voltage stresses across components are high and the circuit structures are complex. The boost three-level DC-DC converter can reduce the voltage stresses across components, but the voltage gain is still as low as the conventional boost converter. The voltage stresses across components are significantly reduced and the theoretical voltage gain can reach $(1+d)/(1-d)$, which is slightly larger than the conventional boost converter. However, the voltage gain is still not enough for fuel cell vehicles. Z-source and quasiZ-source networks are applied to the DC-DC converter to obtain the high-gain, but the voltage stresses of components in the converter are still high. A converter based on a series structure of three Z-source networks is proposed, which can obtain high-gain, wide input voltage range and low stress. However, there are too many inductors and power semiconductors in the circuit, which increases the cost and size of the converter. The converters proposed can achieve high-gain and low voltage stress, but there is a non-common ground structure between the input and output ports of each converter. When the converter is working, there is a high frequency pulsated voltage between the input and output ports, which can cause serious EMI problems. In addition, the main problem is about the voltage feedback for the non-common ground structure. An isolated voltage feedback should be adopted, such as: linear optocoupler, which can increase the complexity of the sampling circuit. The multi-level converters proposed can achieve high-gain and low voltage stresses across components. However, there are too many power semiconductors in the circuit, resulting in increased cost and size. Multiple power switches also increase complexity to the drive circuit and control strategy. The non-isolated converters with coupled-inductors proposed can easily achieve high-gain, reduce the size of the inductor and increase the power density of the converter. However, due to the existence of leakage inductance, additional clamp circuit or absorption circuit should be adopted to absorb the leakage inductance energy, which increases the complexity of the converter.

SIMULATION RESULTS AND ANALYSIS

PARAMETERS DESIGN AND DYNAMIC MODELING

Design Of Inductor And Capacitors In terms of the converter topology, the inductor L can be calculated by (13).

$$L = uL\frac{dt}{di_{,}} \qquad (13)$$

The maximum inductor current and the maximum duty ratio can be obtained when the input voltage is the lowest, that is Uin=25V in the proposed converter. Therefore, the inductor is designed when Uin=25V, UO=200V, f=20kHz and RL=400Ω in this project. Assuming the current ripple of inductor L isΔ IL , hence, the current ripple coefficient of inductor L is γ =ΔIL / IL . In order to avoid excessive inductor current ripple, the ripple rate of inductor current is set as $\gamma \leq 0.4$. When the converter operates in the ON state as shown in Fig. 3.7(a), uL=uin+uc1, dt=d×T=d/f. In the calculation equation of inductance can be obtained as (14).

$$L \geq \frac{d(1-2d)R_L}{4\gamma f} = 750\mu H \qquad (14)$$

Where f is the switching frequency of the converter and d is the duty cycle of the drive signal for power switches Q1 and Q2. When RL=400Ω and UO=200V, the output current IO = UO / RL =0.5A, IL=7.14A can be obtained. When Uin=25V and UO=200V, the peak value of inductor current I_{L_peak} is obtained in equation 15.

$$I_{L\_peak} = I_L + \frac{\Delta L}{2} = I_L + \frac{I_L\gamma}{2} = 8.6A \qquad (15)$$

The energy storage of the magnetic core is calculated as in (4).

$$L.I^2_{L\_peak} = 0.8\,mH\,x\,(8.6)^2 = 59.8\text{mH.A}^2 \qquad (16)$$

Considering the flux density and price, the ferrosilicon aluminum magnetic core is adopted in this project. By referring to magnetic core selection curves of Magnetics company for the iron-silica-aluminum, the 77438 magnetic core is selected for inductor design in this project. The capacitor C can be calculated by using (16). Assuming the voltage ripples of capacitors C1, C2, C3, C4 are $f'U_{C1}$, $f'U_{C2}$, $f'U_{C3}$, $f'U_{C4}$, respectively. In the calculation equation of capacitance can be obtained as (6\17)

$$C = ic\frac{dt}{duc} \qquad (17)$$

$$\begin{cases} C_1 = \dfrac{2dIo}{(1-2d)\Delta U_{C1} f} \\ C_2 = \dfrac{Io}{\Delta U_{C2} f} \\ C_3 = \dfrac{dIo}{\Delta U_{C3} f} \\ C_4 = \dfrac{(1+d)Io}{\Delta U_{C4} f} \end{cases} \qquad (18)$$

Dynamic Modeling Analysis

When the converter operates in the ON state, capacitors C2 and C4 are in parallel as shown. The relationship between C2 and C4 is shown in (7), indicating that there is an invalid variable between C2 and C4.

$$C_2\frac{du_{C2}}{dt}=-C_4\frac{du_{C4}}{dt} \tag{7}$$

In order to eliminate the invalid variable between C2 and C4, the series equivalent resistance r1 is introduced into C2 and C4 loop and equation (7) can be written as (8).

$$C_2\frac{du_{C2}}{dt}=-\frac{u_{C4}-u_{C2}}{r_1} \tag{8}$$

Where the r1 is the equivalent series resistance in C2 and C4 loop, defined as r1 = 0.01Ω. When the converter operates in the OFF state, the series equivalent resistance r2 = 0.01Ω is adopted to eliminate the invalid variable of C1, C2, C3 and C4 loops as shown in Fig. 4(b). After adopting equivalent resistances r1 and r1, the equivalent circuit topology is as shown in Fig.5.1.

$$\begin{cases}\begin{bmatrix}\frac{di_L(t)}{dt}\\ \frac{du_{C1}(t)}{dt}\\ \frac{du_{C2}(t)}{dt}\\ \frac{du_{C3}(t)}{dt}\\ \frac{du_{C4}(t)}{dt}\end{bmatrix}=\begin{bmatrix}0 & \frac{1}{L} & 0 & 0 & 0\\ \frac{-1}{C_1} & 0 & 0 & 0 & 0\\ 0 & 0 & \frac{-1}{r_1C_2} & 0 & 0\\ 0 & 0 & 0 & \frac{-1}{C_3R_L} & \frac{-1}{C_3R_L}\\ 0 & 0 & \frac{1}{C_4r_1} & \frac{-1}{C_4R_L} & \frac{-R_L-r_1}{C_4R_Lr_1}\end{bmatrix}\begin{bmatrix}i_L(t)\\ u_{C1}(t)\\ u_{C2}(t)\\ u_{C3}(t)\\ u_{C4}(t)\end{bmatrix}+\begin{bmatrix}\frac{1}{L}\\ 0\\ 0\\ 0\\ 0\end{bmatrix}u_{in}(t)\\ u_O(t)=[0,0,0,1,1][i_L(t),u_{C1}(t),u_{C2}(t),u_{C3}(t),u_{C4}(t)]^T\end{cases} \tag{21}$$

$$\begin{cases}\begin{bmatrix}\frac{di_L(t)}{dt}\\ \frac{du_{C1}(t)}{dt}\\ \frac{du_{C2}(t)}{dt}\\ \frac{du_{C3}(t)}{dt}\\ \frac{du_{C4}(t)}{dt}\end{bmatrix}=\begin{bmatrix}0 & \frac{2d(t)-1}{L} & 0 & 0 & 0\\ \frac{1-2d(t)}{C_1} & \frac{(r_1+r_2)(d(t)-1)}{C_1r_1r_2} & \frac{1-d(t)}{C_1r_2} & \frac{1-d(t)}{C_1r_2} & \frac{(r_1-r_2)(1-d(t))}{C_1r_1r_2}\\ 0 & \frac{1-d(t)}{C_2r_2} & \frac{r_1-d(t)(r_1+r_2)}{C_2r_1r_2} & \frac{d(t)-1}{C_2r_2} & \frac{d(t)-1}{C_2r_2}\\ 0 & \frac{1-d(t)}{C_3r_2} & \frac{1-d(t)}{C_3r_2} & \frac{(d(t)-1)R_L-r_2}{C_3r_2R_L} & \frac{(d(t)-1)R_L-r_2}{C_3r_2R_L}\\ 0 & \frac{(r_1+r_2)(1-d(t))}{C_4r_1r_2} & \frac{r_1+d(t)(r_2-r_1)}{C_4r_1r_2} & \frac{(d(t)-1)R_L-r_2}{C_4r_2R_L} & \frac{r_1R_Ld(t)-r_1r_2-r_1R_L-r_2R_L}{C_4r_1r_2R_L}\end{bmatrix}\begin{bmatrix}i_L(t)\\ u_{C1}(t)\\ u_{C2}(t)\\ u_{C3}(t)\\ u_{C4}(t)\end{bmatrix}+\begin{bmatrix}\frac{d(t)}{L}\\ \frac{(r_1+r_2)(d(t)-1)}{C_1r_1r_2}\\ \frac{1-d(t)}{C_2r_2}\\ \frac{1-d(t)}{C_3r_2}\\ \frac{(r_1+r_2)(1-d(t))}{C_4r_1r_2}\end{bmatrix}u_{in}(t)\\ u_O(t)=[0,0,0,1,1][i_L(t),u_{C1}(t),u_{C2}(t),u_{C3}(t),u_{C4}(t)]^T\end{cases} \tag{23}$$

$$\begin{bmatrix}\frac{d\tilde{i}_L(t)}{dt}\\ \frac{d\tilde{u}_{C1}(t)}{dt}\\ \frac{d\tilde{u}_{C2}(t)}{dt}\\ \frac{d\tilde{u}_{C3}(t)}{dt}\\ \frac{d\tilde{u}_{C4}(t)}{dt}\end{bmatrix}=\begin{bmatrix}0 & \frac{2D-1}{L} & 0 & 0 & 0\\ \frac{1-2D}{C_1} & \frac{(r_1+r_2)(D-1)}{C_1r_1r_2} & \frac{1-D}{C_1r_2} & \frac{1-D}{C_1r_2} & \frac{(r_1-r_2)(1-D)}{C_1r_1r_2}\\ 0 & \frac{1-D}{C_2r_2} & \frac{r_1-D(r_1+r_2)}{C_2r_1r_2} & \frac{D-1}{C_2r_2} & \frac{D-1}{C_2r_2}\\ 0 & \frac{1-D}{C_3r_2} & \frac{1-D}{C_3r_2} & \frac{(D-1)R_L-r_2}{C_3r_2R_L} & \frac{(D-1)R_L-r_2}{C_3r_2R_L}\\ 0 & \frac{(r_1+r_2)(1-D)}{C_4r_1r_2} & \frac{r_1+D(r_2-r_1)}{C_4r_1r_2} & \frac{(D-1)R_L-r_2}{C_4r_2R_L} & \frac{r_1R_LD-r_1r_2-r_1R_L-r_2R_L}{C_4r_1r_2R_L}\end{bmatrix}\begin{bmatrix}\tilde{i}_L(t)\\ \tilde{u}_{C1}(t)\\ \tilde{u}_{C2}(t)\\ \tilde{u}_{C3}(t)\\ \tilde{u}_{C4}(t)\end{bmatrix}+\begin{bmatrix}\frac{D}{L}\\ \frac{(r_1+r_2)(D-1)}{C_1r_1r_2}\\ \frac{1-D}{C_2r_2}\\ \frac{1-D}{C_3r_2}\\ \frac{(r_1+r_2)(1-D)}{C_4r_1r_2}\end{bmatrix}\tilde{u}_{in}(t)$$

$$G_{d\rightarrow uo}(s)=\left.\frac{\tilde{u}_o(s)}{\tilde{d}(s)}\right|_{\tilde{u}_{in}(s)=0}=\frac{-1.225\times10^{9}s^{4}-2.61\times10^{14}s^{3}+4.341\times10^{19}s^{2}+1.522\times10^{24}s-1.103\times10^{22}}{s^{5}+6.689\times10^{5}s^{4}+1.266\times10^{11}s^{3}+1.112\times10^{16}s^{2}+4.511\times10^{20}s+1.3\times10^{20}} \tag{26}$$

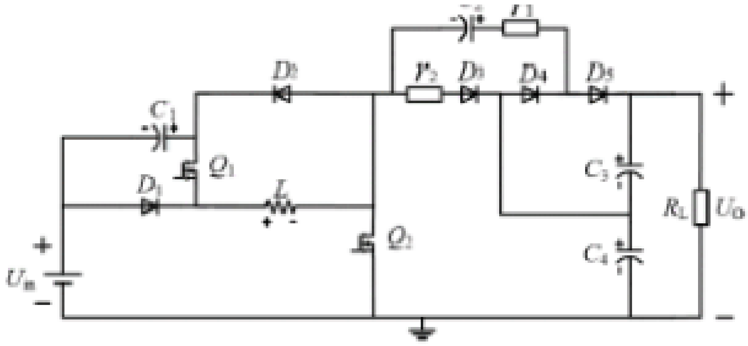

Fig. 5.15.1 Circuit topology after adopting equivalent resistances r1 and r2

The state-space averaging method is used to model the converter in CCM. uin(t) is the input variable, uo(t) is the output variable and d(t) is the control variable. iL(t), uC1(t), uC2(t), uC3(t), uC4(t) are the state variables of inductor L and capacitors C1, C2, C3, C4 respectively. When the converter operates in the ON state and the working time is dT, the state space equation is obtained as (21). When the converter operates in the OFF state and the working time is (1−d)T, the state space equation is obtained as (22). In terms of (21) and (22), the state space averaging equation over a switching period can be obtained as shown in (23). Equation (24) is obtained when all variables are written as the sum of DC and small signals components. By substituting (24) into (23) and removing the DC components, the small signal model of the converter is obtained as shown in (25)

$$\begin{cases} i_L(t)=I_L+\tilde{i}_L(t) \\ u_{C1}(t)=U_{C1}+\tilde{u}_{C1}(t) \\ u_{C2}(t)=U_{C2}+\tilde{u}_{C2}(t) \\ u_{C3}(t)=U_{C3}+\tilde{u}_{C3}(t) \\ u_{C4}(t)=U_{C4}+\tilde{u}_{C4}(t) \\ u_{in}(t)=U_{in}+\tilde{u}_{in}(t) \\ u_O(t)=U_O+\tilde{u}_O(t) \\ d(t)=D+\tilde{d}(t) \end{cases} \quad (24)$$

where IL, UC1, UC2, UC3, UC4, Uin, UO, D are the DC steady-state components of the corresponding variables. iL(t) uC1(t) uC2(t) uC3(t) uC4(t) uin(t) uO(t) d(t) are the small signal components of the corresponding variables.

p-ISSN: 2348-6848
e-ISSN: 2348-795X
Vol. 8 Issue 12
December 2021

TABLE I DESIGN PARAMETERS OF THE CONVERTER

Parameters	**Values**
Rated power P	100W
Input voltage U_{in}	25V-80 V
Rated output Voltage U_0	200V
Rated load resistance R_L	400Ω
Switching frequency f	20kHz
Inductor L	800μH
Capacitors C_1,C_2,C_3,C_4	470μF
Power switches Q_1,Q_2	DXTK102N30P
Diodes D_1,D_2,D_3,D_4,D_5	DSEC 60-03A

The design parameters of the converter are shown in Table I. When Uin=25V and UO=200V, in terms of (25) and Table II, the transfer functions of control-to-output are obtained as shown in equation (26). The dynamic model of the proposed converter in (26) is written into the pole-zero form as shown in (27). In order to simplify analysis, the original model in (27) is reduced from 5 to 4 in order to obtain the simplified model in (28). By appropriate pole-zero elimination method, the (s+3.135×105) in numerator and the (s+4.283 ×105) in denominator are eliminated in equation(27). The BODE diagram curves of (27) and (28) are shown in Figure 5.2. From Fig.5.2, it can be seen that the original and simplified model curves are approximately the same. Therefore, the PI controller is designed based on (28).

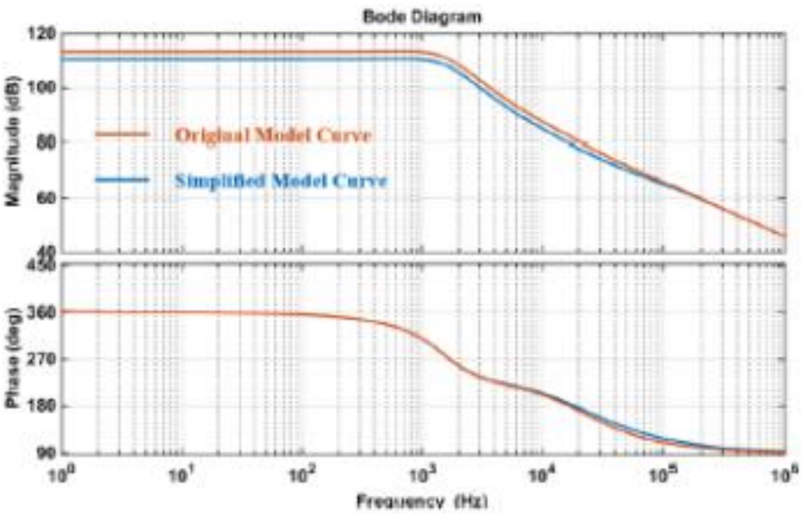

Fig.5.2. Bode diagram of the proposed converter.

The PI controller is designed in order to achieve stable operation for the converter system. The block diagram of the closed-loop control system for the converter is shown in Fig.5.35.3. GFB(s) is the feedback network transfer function. The actual prototype adopts the Hall sensor to collect the output voltage. Gd uo(s) is the transfer function of the converter from control to output. GPI(s) is the transfer function of the PI controller as shown in (29). The converter system can obtain good dynamic and static performance by using the PI controller.

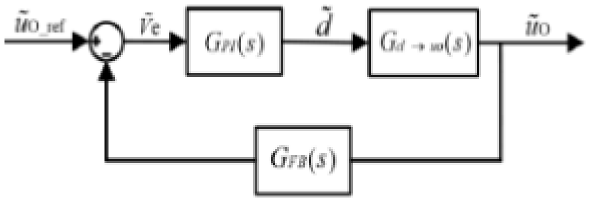

Fig.5.3. The block diagram of the closed-loop control system of the converter

$$G_{ZPK}(s)=\frac{-1.2247\times10^{9}(s+3.135\times10^{5})(s-1.307\times10^{5})(s+3.031\times10^{4})(s-0.007247)}{(s+4.283\times10^{5})(s+1.165\times10^{5})(s+0.2883)(s^{2}+1.242\times10^{4}s+9.04\times10^{7})} \quad (27)$$

$$\hat{G}_{ZPK}(s)=\frac{-1.2247\times10^{9}(s-1.307\times10^{5})(s+3.031\times10^{4})(s-0.007247)}{(s+1.165\times10^{5})(s+0.2883)(s^{2}+1.242\times10^{4}s+9.04\times10^{7})} \quad (28)$$

$$G_{PI}(s)=K_P+\frac{K_I}{s} \quad (29)$$

where the KP is the proportional coefficient and KI is the integral coefficient. For this work, Kp = 0.000008 and KI = 0.000005. By using the PI controller, the Bode diagram of the converter closed-loop system is shown in Fig.5.45.4. The phase margin of the closed-loop system is 53.7°, which indicates the system can achieve stable operation.

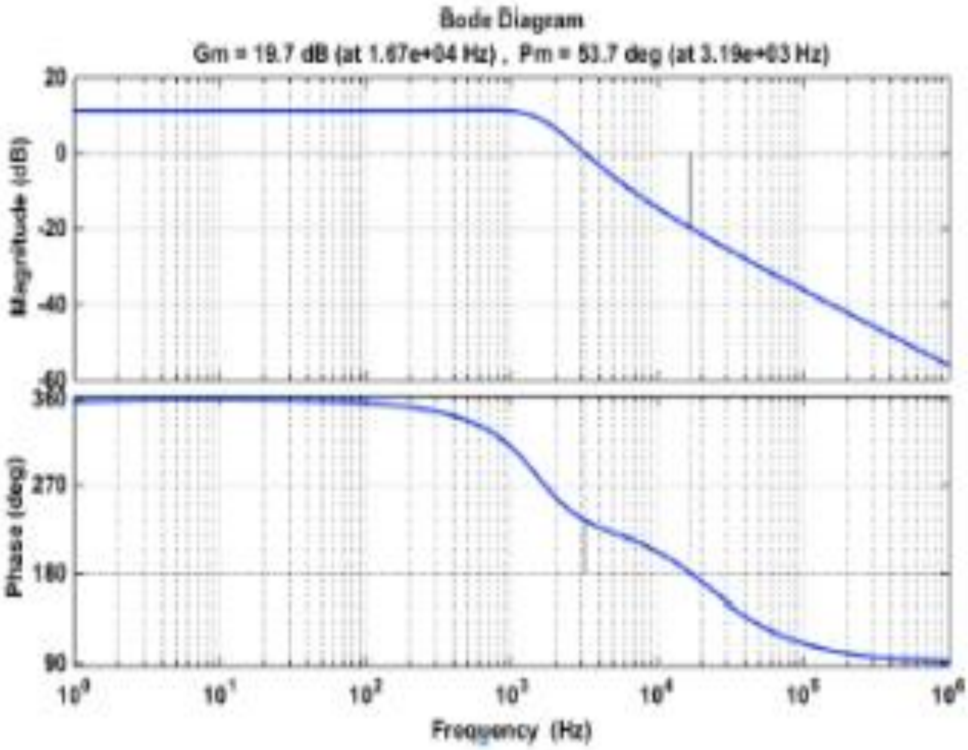

Fig. 5.4. The BODE diagram of a closed-loop system for the converter.

In terms of practicality and stability, the bilinear transformation method is adopted to design the digital controller in this project. By using bilinear transformation method, the relation between variable s in s domain and variable z in z domain is shown in (30) as follows [32].

$$s=\frac{2}{T_s}\cdot\frac{z-1}{z+1} \qquad (30)$$

where Ts is the sampling period of a discrete system. Ts= 0.00005s in this project. In terms of (29) and (30) above, by using bilinear transformation method, the PI controller equation in z domain is obtained as (31).

$$\frac{d(z)}{Ve(z)}=\frac{(K_P+\frac{T_s}{2}\cdot K_I)\cdot z+\frac{T_s}{2}\cdot K_I-K_P}{z-1} \qquad (31)$$

where Ve(z) is the input error voltage of the PI controller in the z domain. d(z) is the output duty cycle of the PI controller in the z domain. The values of KI, KP and Ts above are substituted into equation (31) to obtain (32) as follows.

$$\frac{d(z)}{Ve(z)}=\frac{8\times10^{-6}+7.99\times10^{-6}\cdot z^{-1}}{1-z^{-1}} \qquad (32)$$

Equation (32) is transformed into the difference equation as shown in (33), which is the expression of the discrete PI controller. According to (33), a PI control program can be written in a controller to realize closed-loop control and ensure the stability of the converter system.

$$d(k)=d(k-1)+8\times10^{-6}\cdot Ve(k)+7.99\times10^{-6}\cdot Ve(k-1) \qquad (33)$$

5.3. Block diagram of the proposed system

5.3.1. Simulation results of converter during Drive voltage and Load current

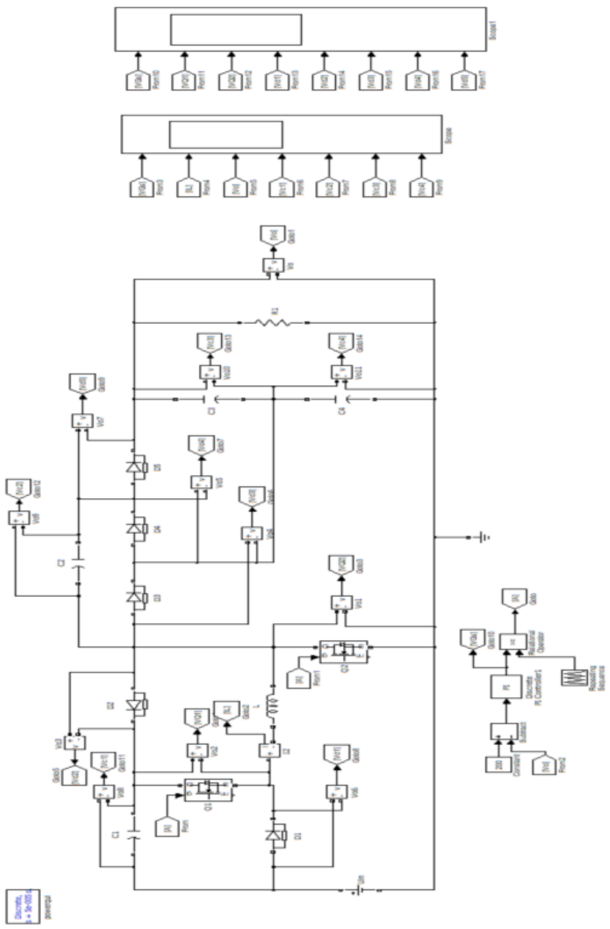

p-ISSN: 2348-6848
e-ISSN: 2348-795X
Vol. 8 Issue 12
December 2021

Fig.5.5. Simulation results of converter during Drive voltage and Load current

In order to verify the effectiveness of the proposed converter, a simulation model is built for the converter system and simulation parameters are shown in Table I. When the input voltage is U_{in}=25 V and the reference output voltage is set as U_{O_ref} =200 V, the simulation results are shown in Fig.5.55.6. From Fig5.5.5.6 and fig 5.7, the inductor current IL is 7.5 A, which is consistent with the theoretical calculation result. The output voltage UO has been stable at 200 V. The voltage stresses across all capacitors and power semiconductors are as follows: $U_{Q1}=U_{C1}=U_{D1} \approx 75$ V $U_{Q2}=U_{C2}=U_{C3}=U_{C4}=U_{D2}=U_{D3}=U_{D4}$=UD5 ≈ 100 V, which are consistent with the theoretical calculation results obtained

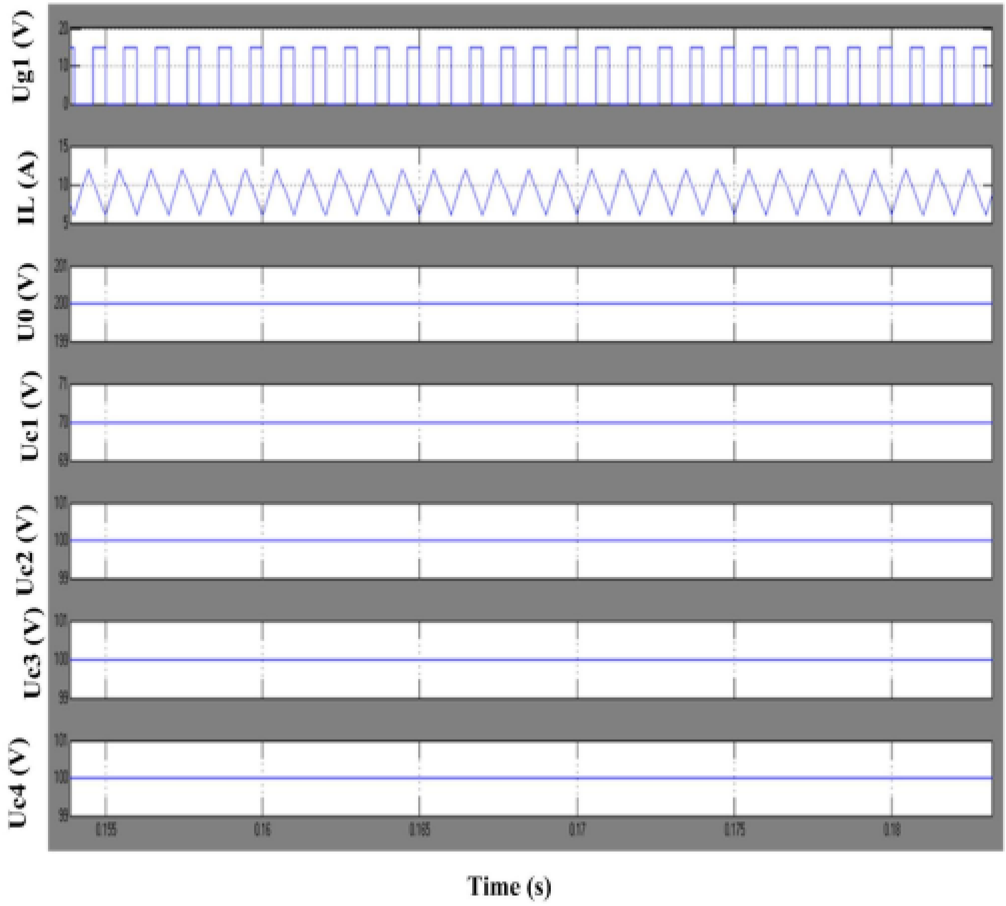

Fig.5.6. Simulation results of converter during Drive voltage Ugs, inductor current IL, output voltage UO and voltage stresses across C1, C2, C3, C4.

The simulation results show that the proposed converter has advantages of high-gain and low voltage stresses across components, which verifies the effectiveness of the circuit topology. The dynamic simulation results of the converter are shown in Figure 5.65.7. When the simulation time is 1s, the input voltage of the converter Uin starts to drop from 60V and finally drops to 25V, with a total time of 14s. When the simulation time is 16s, the output current IO changes suddenly from 250mA to 500mA and remains 200ms. Then the IO changes suddenly from 500mA to 250mA. From Fig.5.7, it can be concluded that the converter can maintain the output voltage stable around the reference voltage under the input voltage and load disturbance. The system can obtain a good anti-interference performance.

p-ISSN: 2348-6848
e-ISSN: 2348-795X
Vol. 8 Issue 12
December 2021

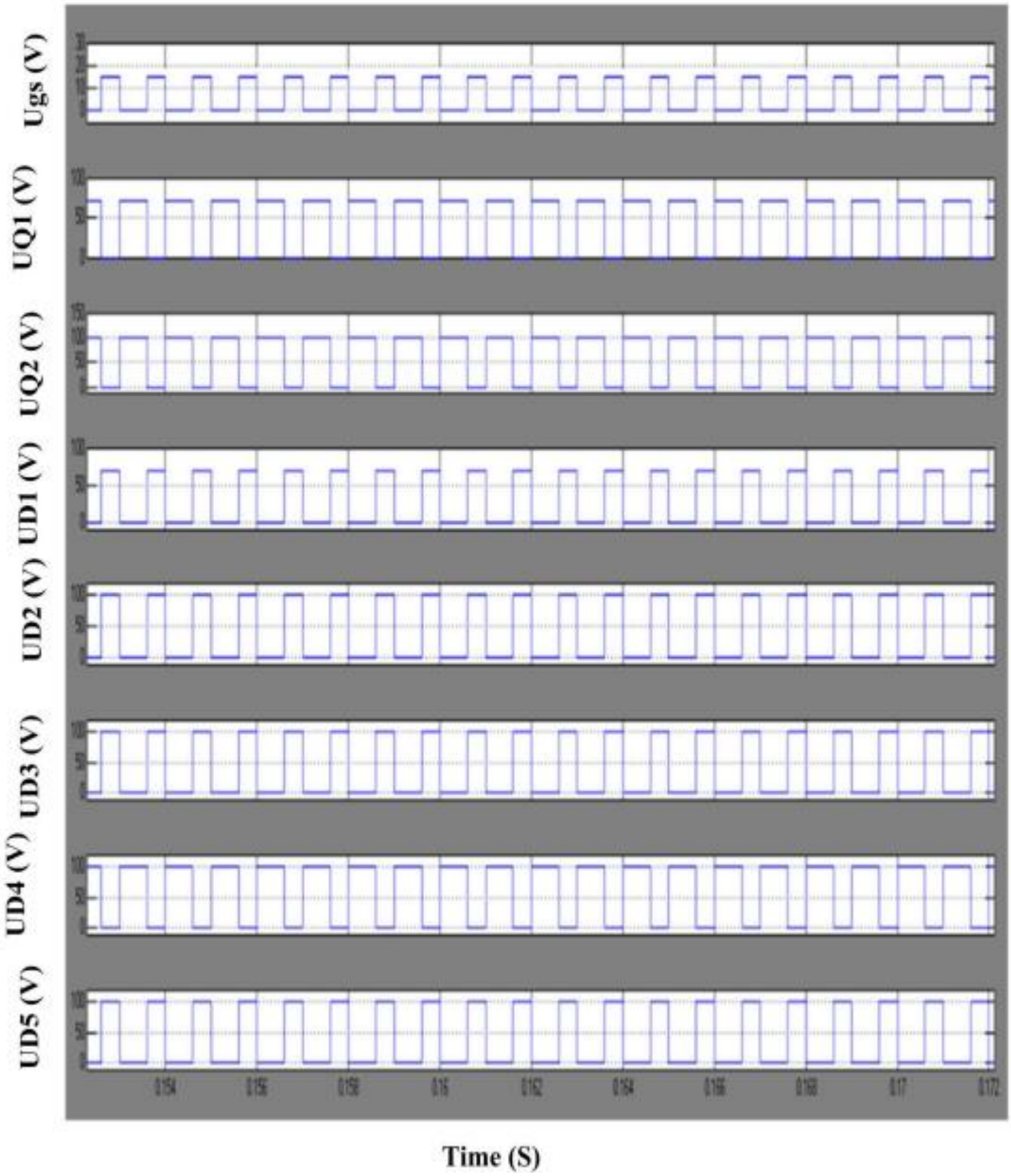

Fig.5.7. Simulation results of converter during Drive voltage Ugs , voltage stresses across Q1 and Q2, voltage stresses across D1, D2, D3, D4, D5.

p-ISSN: 2348-6848
e-ISSN: 2348-795X
Vol. 8 Issue 12
December 2021

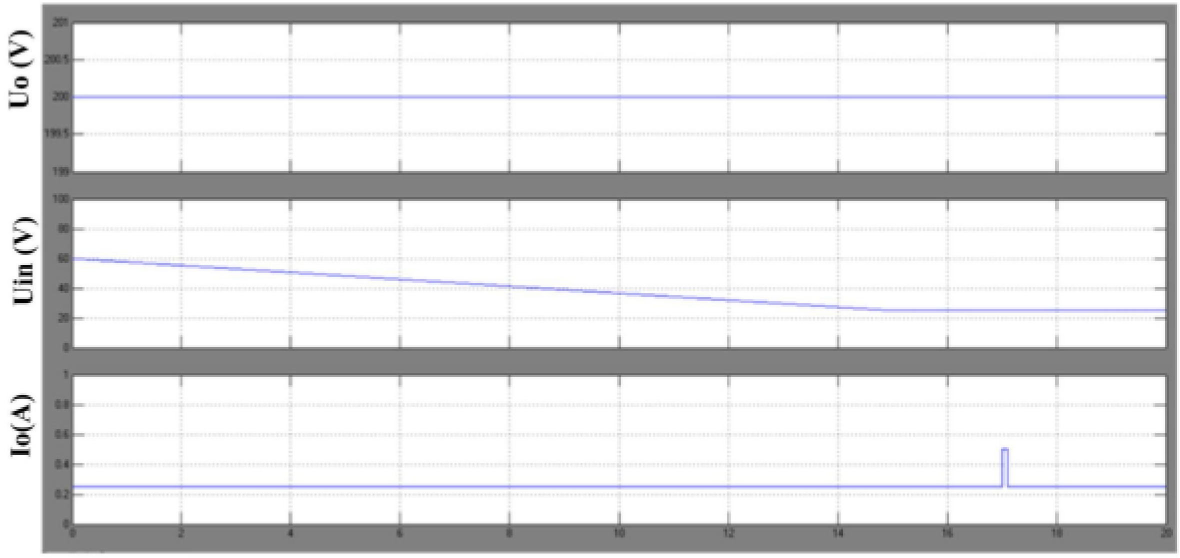

CONCLUSION

This project presents a non-isolated DC-DC converter topology for fuel cell vehicles. The proposed converter can obtain high-gain and wide input voltage range. The voltage gain can reach 2(1−d)/(1−2d) and duty cycle d<0.5 while achieving high-gain. The voltage stresses across components are less than half of the output voltage, which is beneficial to reduce the size and cost of the converter. In addition, the circuit topology is a common ground structure, which can avoid EMI and safety problems. The converter can always maintain the stability of the output voltage by closed-loop control. There is no voltage overshoot and impulse current during the soft-start process by adopting the soft-start program. Under the rated state, the measured maximum efficiency of the prototype is 93.1%. The proposed converter is suitable for fuel cell vehicles.

REFERENCES

[1] G. Du, W. Cao S. Hu Z. Lin and T. Yuan “Design and Assessment of an Electric Vehicle Powertrain Model BaXCV Z+sed on Real-World Driving and Charging Cycles ” IEEE Trans. Veh. Technol., vol. 68, no. 2, pp. 1178-1187, Feb. 2019.

[2] Z. Geng, Q. Chen, Q. Xia D. S. Kirschen and C. Kang “Environmental Generation Scheduling Considering Air Pollution Control Technologies and Weather Effects ” IEEE Trans. Power Syst., vol. 32, no. 1, pp. 127-136, Jan. 2017.

[3] H. Bi P. Wang and Y. Che “A Capacitor Clamped H-Type Boost DC-DC Converter With Wide Voltage-Gain Range for Fuel Cell Vehicles ” IEEE Trans. Veh. Technol., vol. 68, no. 1, pp. 276-290, Jan. 2019.

[4] L. Li, S. Coskun, F. Zhang R. Langari and J. Xi “Energy Management of Hybrid Electric Vehicle Using Vehicle Lateral Dynamic in Velocity Prediction ” IEEE Trans. Veh. Technol., vol. 68, no. 4, pp. 3279-3293, Apr.2019.

[5] N. Elsayad, H. Moradisizkoohi, and O. A. Mohammed “A Single-Switch Transformerless DC-DC Converter With Universal Input Voltage for Fuel Cell Vehicles: Analysis and Design ” IEEE Trans. Veh. Technol., vol. 68, no. 5, pp. 4537-4549, Mar. 2019.

[6] O. Hegazy, J. Van Mierlo and P. Lataire “Analysis, Modeling, and Implementation of a Multidevice Interleaved DC-DC Converter for Fuel Cell Hybrid Electric Vehicles ” IEEE Trans. Power Electron., vol. 27, no. 11, pp. 4445-4458, Nov. 2012.

[7] Z. Qun and F. C. Lee “High-efficiency, high step-up DC-DC converters ” IEEE Trans. Power Electron., vol. 18, no. 1, pp. 65-73, Jan. 2003.

p-ISSN: 2348-6848
e-ISSN: 2348-795X
Vol. 8 Issue 12
December 2021

[8] B. Gu, J. Dominic, J.-S. Lai Z. Zhao and C. Liu “High Boost Ratio Hybrid Transformer DC–DC Converter for Photovoltaic Module Applications ” IEEE Trans. Power Electron., vol. 28, no. 4, pp. 2048-2058, Apr. 2013.
[9] C. T. Pan and C. M. Lai “A High-Efficiency High Step-Up Converter With Low Switch Voltage Stress for Fuel-Cell System Applications ” IEEE Trans. Ind. Electron., vol. 57, no. 6, pp. 1998-2006, Jun. 2010.
[10] G. A. L. Henn, R. N. A. L. Silva, P. P. Praça, L. H. S. C. Barreto, and D. S. Oliveira “Interleaved-Boost Converter With High Voltage Gain ” IEEE Trans. Power Electron., vol. 25, no. 11, pp. 2753-2761, Nov. 2010
[11] F. Wen J. Shabani and E. Tutuc “Josephson Junction Field-Effect Transistors for Boolean Logic Cryogenic Applications ” IEEE Trans. Electron Devices., vol. 66, no. 12, pp. 5367-5374, Dec. 2019.
[12] F. L. Tofoli, D. de Castro Pereira; W. J. de Paula, and D. de Sousa Oliveira Junior “Survey on non-isolated high-voltage step-up dc–dc topologies based on the boost converter ” IET Power Electron., vol. 8, no. 10, pp. 2044-2057, Sep. 2015.
[13] F. L. Luo and H. Ye, “Positive output cascade boost converters ” in Proc. IEE Proc. Electr. Power Appl., vol. 151, no. 5, pp. 590-606, Sep. 2004.
[14] J. P. Rodrigues, S. A. Mussa, M. L. Heldwein and A. J. Perin “Three-Level ZVS Active Clamping PWM for the DC-DC Buck Converter ” IEEE Trans. Power Electron., vol. 24, no. 10, pp. 2249-2258, Oct. 2009.
[15] Y. L. Sheng L. T. Juu and C. J. Fuh “Transformerless DC–DC Converters With High Step-Up Voltage Gain ” IEEE Trans. Ind. Electron., vol. 56, no. 8, pp. 3144-3152, Aug. 2009. [16] J. Anderson and F. Z. Peng “A Class of Quasi-Z-Source Inverters ” in Proc. IEEE Ind. Appl. Soc., Oct. 2008, pp. 1-7.
[17] V. P. Galigekere and M. K. Kazimierczuk “Analysis of PWM Z-Source DC-DC Converter in CCM for Steady State ” IEEE Trans. Circuits Syst. I, Reg. Papers., vol. 59, no. 4, pp. 854-863, Apr. 2012.
[18] G. Zhang, B. Zhang, Z. Li, and D. Qiu “A 3-Z-Network Boost Converter ” IEEE Trans. Ind. Electron., vol. 62, no. 1, pp. 278-288, Jan. 2015.
[19] M. K. Nguyen, T. D. Duong and Y. C. Lim “Switched-Capacitor-Based Dual-Switch High-Boost DC–DC Converter ” IEEE Trans. Power Electron., vol. 33, no. 5, pp. 4181-4189, May. 2018.
[20] R. J. K. Prasana, S. Ramprasath and N. Vijayasarathi “Design and analysis of hybrid DC-DC boost converter in continuous conduction mode ” in Proc. IEEE Int. Conf. Circuit, Power Comput. Technol., Power and Computing Technol., Mar. 2016, pp. 1-5.
[21] X. Hu and C. Gong, “A High Gain Input-Parallel Output-Series DC/DC Converter With Dual Coupled Inductors ” IEEE Trans. Power Electron., vol. 30, no. 3, pp. 1306-1317, Mar. 2015
[22] A. Rajaei, R. Khazan, M. Mahmoudian and M. Mardaneh “A Dual Inductor High Step-Up DC/DC Converter Based on the Cockcroft–Walton Multiplier ” IEEE Trans. Power Electron., vol. 33, no. 11, pp. 9699-9709, Nov. 2018.
[23] X. B. Ruan, B. Li, Q. H. Chen, T. Siew-Chong, and C. K. Tse, “Fundamental Considerations of Three-Level DC–DC Converters: Topologies Analyses and Control ” IEEE Trans. Circuits Syst. I, Reg. Papers., vol. 55, no. 11, pp. 3733-3743, Dec. 2008.
[24] L. Sun, F. Zhuo, F. Wang, and T. Zhu, “A novel topology of high voltage and high power bidirectional ZCS DC-DC converter based on serial capacitors ” in Proc. IEEE Appl Power Electron Conf Expo APEC, Mar. 2016, pp. 810-815.
[25] J. H. Lee T. J. Liang and J. F. Chen “Isolated Coupled-Inductor-Integrated DC-DC Converter With Nondissipative Snubber for Solar Energy Applications ” IEEE Trans. Ind. Electron., vol. 61, no. 7, pp. 3337-3348, Jul. 2014.

[26] C. S. Kuen L. T. Juu C. J. Fuh and Y. L. Sheng "Novel High Step-Up DC-DC Converter for Fuel Cell Energy Conversion System," IEEE Trans. Ind. Electron., vol. 57, no. 6, pp. 2007-2017, Jun. 2010.
[27] Y. P. Hsieh, J. F. Chen, T. J. Liang, and L. S. Yang "A Novel High Step-Up DC-DC Converter for a Microgrid System " IEEE Trans. Power Electron., vol. 26, no. 4, pp. 1127-1136, Apr. 2011. [28] P. Wang, L. Zhou, Y. Zhang, J. Li, and M. Sumner, "Input-Parallel Output-Series DC-DC Boost Converter With a Wide Input Voltage Range For Fuel Cell Vehicles " IEEE Trans. Veh. Technol., vol. 66, no. 9, pp. 7771-7781, Sep. 2017.
[29] Y. Zhang, L. Zhou M. Sumner and P. Wang "Single-Switch, Wide Voltage-Gain Range, Boost DC–DC Converter for Fuel Cell Vehicles " IEEE Trans. Veh. Technol., vol. 67, no. 1, pp. 134-145, Jan. 2018.
[30] Y. Zhang J. Shi L. Zhou and J Li "Wide Input-Voltage Range Boost Three-Level DC–DC Converter With Quasi-Z Source for Fuel Cell Vehicles " IEEE Trans. Power Electron., vol. 32, no. 9, pp. 6728-6738, Sep. 2017.
[31] Y. Shindo M. Yamanaka and H. Koizumi "Z-source DC-DC converter with cascade switched capacitor " in Proc. IEEE Ind. Electron. Soc., Nov. 2011, pp. 1665-1670.
[32] A. Narayana "State-space approach to the bilinear transformation and some extensions " IEEE Trans. Educ., vol. 34, no. 1, pp. 139-142, Feb. 1991.